5-31-2022

Formation of Gaseous Peptide Ions from Electrospray Droplets: Competition between the Ion Evaporation Mechanism and Charged Residue Mechanism.

Elnaz Aliyari

Lars Konermann

Formation of Gaseous Peptide Ions from Electrospray Droplets: Competition between Ion Evaporation Mechanism (IEM) and Charged Residue Mechanism (CRM)

Elnaz Aliyari and Lars Konermann*

Department of Chemistry, The University of Western Ontario, London, Ontario, N6A 5B7, Canada

* To whom correspondence should be addressed. E-mail: konerman@uwo.ca.

Funding was provided by the Natural Sciences and Engineering Research Council of Canada (RGPIN-2018-04243).

ABSTRACT: The transfer of peptide ions from solution into the gas phase by electrospray ionization (ESI) is an integral component of mass spectrometry (MS)-based proteomics. The mechanisms whereby gaseous peptide ions are released from charged ESI nanodroplets remain unclear. This is in contrast to intact protein ESI, which has been the focus of detailed investigations using molecular dynamics (MD) simulations and other methods. Under acidic LC/MS conditions, many peptides carry a solution charge of 3+ or 2+. Because of this pre-existing charge and their relatively small size, prevailing views suggest that peptides follow the ion evaporation mechanism (IEM). The IEM entails analyte ejection from ESI droplets, driven by electrostatic repulsion between analyte and droplet. Surprisingly, recent peptide MD investigations reported a different behavior, i.e., the release of peptide ions via droplet evaporation to dryness which represents the hallmark of the charged residue mechanism (CRM). Here we resolved this conundrum by performing MD simulations on a common model peptide (bradykinin) in Rayleigh-charged aqueous droplets. The primary focus was on pH 2 conditions (bradykinin solution charge = 3+), but we also verified that our MD strategy captured pH-dependent charge state shifts seen in ESI-MS experiments. In agreement with earlier simulations, we found that droplets with initial radii of 1.5 nm to 3 nm predominantly release peptide ions via the CRM. In contrast, somewhat larger radii (4 nm to 5 nm) favor IEM behavior. It appears that these are the first MD data to unequivocally demonstrate the viability of peptide IEM events. Electrostatic arguments can account for the observed droplet size dependence. In summary, both CRM and IEM can be operative in peptide ESI-MS. The prevalence of one over the other mechanism depends on the droplet size distribution in the ESI plume.

Introduction

Electrospray ionization (ESI) mass spectrometry (MS) has become indispensable for numerous analytical applications.[1] The impact of ESI-MS has been particularly pronounced in the area of proteomics. Some proteomics experiments involve intact protein analyses.[2-4] However, a more widely used approach is the analysis of proteolytic peptides by liquid chromatography (LC) and ESI-MS.[5, 6] In these bottom-up experiments, peptides are desalted and separated on a reverse-phase column, typically using a water/acetonitrile gradient with ~0.1% formic acid. The LC eluate is then infused into the ESI source.[7-10] The acidic LC mobile phase is an "ESI-friendly" solvent that provides high signal intensity and stability.[11-13]

The ESI process commences with charged droplets that emanate from a Taylor cone at the emitter outlet.[14-16] These droplets undergo solvent evaporation and jet fission,[17] culminating in progeny droplets with radii of a few nm.[11] Throughout this evaporation/fission cascade the net droplet charge stays close to the Rayleigh limit z_R, defined as[11, 18-20]

$$z_R = 8\pi/e \times (\varepsilon_0 \gamma r^3)^{1/2} \qquad (1)$$

where r = droplet radius, γ = surface tension, e = elementary charge. Three main models have been proposed for the release of gaseous analyte ions (typically $[M + zH]^{z+}$) from ESI nanodroplets. (1) According to the ion evaporation mechanism (IEM),[21-24] ions get ejected from the droplet. Driving force for these IEM events is the electrostatic repulsion between the analyte ion and other charges in the droplet. (2) The charged residue mechanism (CRM)[11, 19, 25] describes a scenario where analyte ions are released upon droplet evaporation to dryness. (3) The chain ejection mechanism (CEM) applies to unfolded proteins and other disordered polymers. It involves gradual expulsion via intermediate structures where droplets carry polymer tails that protrude into the vapor phase.[26-28] In addition to these mechanisms, various hybrid scenarios may exist.[24, 29-31]

The question which ESI mechanism applies under a given set of conditions remains controversial.[31-39] Here we focus on the two models with the longest history, i.e., the IEM[21] and the CRM[25]. Prevailing views[3, 11, 40] suggest that the IEM applies to analytes that are small and already charged in solution.[21, 22] The CRM is believed to be operative for analytes that are large and compact, such as globular proteins.[11, 19, 39] However, the IEM vs. CRM distinction on the basis of analyte size is contentious. Some studies suggested a size cut-off in the range of a few kDa,[19, 41] while others proposed values as low as 100 Da,[39] or as high as 5 MDa.[42] This disparity highlights the need for additional investigations.

Recent years have witnessed a renaissance of ESI mechanistic research that has been fueled, in part, by molecular dynamics (MD) simulations of nanodroplets.[24, 26, 27, 43-55] MD studies on small ions confirmed the viability of IEM events,[26, 43-45, 47] while various globular proteins showed CRM behavior.[26] It was also demonstrated that even intact proteins can follow the IEM, provided that they are highly charged in solution (because the IEM relies on electrostatic repulsion) while maintaining a compact structure (because unfolding would promote the CEM).[24]

Unlike intact proteins, the mechanism of peptide ESI has received relatively little attention. This is surprising, considering that peptides are the central analytes in bottom-up proteomics.[5-10, 13] In most LC/ESI-MS workflows, peptides are generated by tryptic digestion. Trypsin cleaves after Arg and Lys (unless followed by Pro),[5, 56] generating peptides with ~10 residues.[8, 57-60] Peptide protonation in solution is promoted by the acidic LC mobile phase and by the presence of at least two basic sites, i.e., the N-terminus and the C-terminal Arg or Lys.[8, 12] Solution charge generally tends to be a poor predictor of ESI charge states,[61-63] but for tryptic peptides at acidic pH, the dominant ESI charge states (3+ and 2+) happen to resemble the charge in solution.[10]

Compared to intact proteins, tryptic peptides are relatively small. As noted above, small size and the presence of a net charge are expected to favor IEM behavior.[11, 19, 41] Accordingly, it is often

implied that peptides follow the IEM.[13, 36, 64, 65] Surprisingly, MD simulations on various 3+ peptides in aqueous droplets with ~3 nm radii did not confirm this expectation. Those studies suggested that gaseous peptide ions (with 9,[53] 11,[49] or 21 residues[66]) are instead formed via droplet evaporation to dryness, consistent with the CRM. IEM behavior was observed in simulations on $GlyGly^+$,[67] but that work focused on nanojets, such that the relevance for typical ESI nanodroplets is unclear. In summary, much remains to be learned about the ESI behavior of peptides.

To shed light on peptide ESI events, the current study took a fresh look at the release of $[M + zH]^{z+}$ peptide ions from ESI nanodroplets using MD simulations. As model compound we chose bradykinin (RPPGFSPFR, monoisotopic mass 1059.56 Da), a peptide that has been the focus of many earlier MS investigations.[53, 61, 68-72] Bradykinin is widely used for benchmarking MS performance, particularly in a proteomics context. It resembles a tryptic peptide because of its size (9 residues), the presence of a C-terminal Arg, and the formation of 3+ and 2+ ions during ESI.[8, 57-60] Bradykinin biosynthesis involves hydrolysis of kininogen by plasma kallikrein, a trypsin-like serine protease.[73] Despite the use of water/acetonitrile in LC/ESI-MS,[7-10, 13] we studied bradykinin in aqueous droplets. This is because organic cosolvents evaporate more quickly than water, such that the final ESI nanodroplets contain a much higher water percentage than the initial solution.[74-77] Aqueous droplets are particularly relevant for peptides that are relatively hydrophilic (such as bradykinin) because these species elute early, when the acetonitrile content of the LC gradient is low.[7] Our data reveal that both the IEM and the CRM are viable ESI mechanisms for bradykinin. The two pathways are in kinetic competition with one another. IEM behavior is prevalent under acidic conditions. However, the ejection electrostatics are favorable only for a certain droplet size range. Our findings reconcile earlier reports of peptide CRM behavior[49, 53, 66] with the traditional expectation that peptides follow the IEM.[13, 36, 64, 65]

Methods

ESI-MS Experiments. Bradykinin acetate salt was from Sigma (St. Louis, MO). Samples with peptide concentration of 5 μM were prepared in LC grade water. Formic acid or ammonium hydroxide were used to adjust the bulk solution pH to 2, 7, or 10. ESI mass spectra were recorded on a Synapt G2 time-of-flight instrument (Waters, Milford, MA) in positive ion mode. Solutions were electrosprayed at +2.8 kV using a standard Z-spray ESI source, with syringe pump infusion at 5 μL min^{-1}. The experiments used gentle source conditions, with a cone voltage of 5 V, and source/desolvation temperatures of 30 °C and 40 °C, respectively. Average *z* values were calculated by considering all peptide charge states, including the -H_2O signals of 3+ ions.

MD Simulations. ESI droplet simulations in positive ion mode were performed using Gromacs 2018.[78] Bradykinin coordinates were initially generated in an extended random conformation using Pymol. Spherical water droplets with initial radii r_0 between 1.5 nm and 5 nm (~420 to ~17300 water molecules) were built around the peptide. The TIP4P/2005 water model[79] was used because it reproduces the surface tension and various other physical water properties over a wide temperature range.[80] Simulations used the CHARMM36 force field,[81] which has been shown to perform well for protein ESI simulations.[26] Na^+ ions were inserted in random positions to bring the initial net droplet charge close to the Rayleigh limit, calculated from eq. 1 with $\gamma = 0.05891$ N m^{-1} for water.[82] For a radius of 1.5 nm the initial droplet charge was 6+, while for 5 nm it was 40+. Other droplet radii (and initial droplet charges) were 4.5 nm (34+), 4.0 nm (29+), 3.5 nm (23+), 3.0 nm (18+), and 2.0 nm (10+). These droplet sizes are in the range of "late" nanodroplets in the ESI plume from which analyte ions are liberated into the gas phase.[11] The use of Na^+ circumvents computational difficulties associated with the Grotthuss diffusion of H^+.[83] Following steepest descent energy minimization, 75 ns MD runs were performed at 370 K using trajectory stitching, where evaporated water and Na^+

were eliminated in 250 ps intervals to speed up the simulations.[26] Bond constraints allowed the use of a relatively long integration step (2 fs).[84] Temperature control was achieved using the Nosé-Hoover thermostat. At least five independent runs were performed for each condition, using different initial atom velocities and Na^+ positions. The three X-Pro peptide bonds underwent occasional *cis-trans* isomerization, a process that also occurs in experiments.[69] The dominant isomers were *trans*/*trans*/*trans* and *trans*/*cis*/*trans* (determined using Pymol dihedral angle measurements), consistent with computational[53] and NMR[85] investigations on bradykinin.

Protonation Patterns for MD Simulations. ESI simulations require a judicious choice of analyte titration pattern within the droplet, keeping in mind that the charge of titratable sites depends on pH (Figure S1). The pH in ESI droplets can differ from that of the bulk analyte solution.[55, 86-90] Reasons for such discrepancies include water oxidation in the source ($2\ H_2O \rightarrow 4\ H^+ + O_2 + 4e^-$).[91] Also, solvent evaporation in the ESI plume increases the concentration of solutes, including H^+ or OH^-.[87] As a result, droplets generated at pH ≤ 7 can be expected to be more acidic than the initial solution.[86] The trend for alkaline solutions is less clear, because pH might go up or down depending on whether OH^- enrichment or electrolytic acidification dominates. pH is a concept that assumes bulk solution equilibria. Such considerations may not be appropriate for shrinking ESI droplets which represent a confined non-equilibrium environment. It has been suggested that excess protons accumulate at the droplet surface, such that acidification of the interior (where analytes reside much of the time) will be less pronounced. Also, titration events can be relatively slow. Carboxylate (Asp^-/Glu^-/C-terminus$^-$) protonation takes place with $k \approx 4.5 \times 10^{10}\ M^{-1}\ s^{-1}$.[92] This corresponds to reaction times of $(0.001\ M \times k)^{-1} \approx 20$ ns at pH 3, ~200 ns at pH 4, or ~2000 ns at pH 5. These time scales are comparable to the final stages of the ESI process,[11] suggesting that titration reactions may lag behind as the droplet pH changes. Droplet-mediated rate enhancements can further complicate the situation.[93] Overall,

the extent of pH changes within ESI droplets and the corresponding implications for analyte titration patterns remain poorly understood. Our MD simulations took a simplistic approach and approximated bradykinin titration patterns based on bulk solution pH (Figure S1). Importantly, ESI-induced pH changes are irrelevant at pH 2, because bradykinin is fully protonated at this pH (Figure S1) such that additional acidification would leave the peptide charge unchanged. Bradykinin at pH 2 was modeled with a 3+ net charge [$nt^{+}R^{+}PPGFSPFR^{+}ct^{0}$], where "nt" and "ct" indicate N- and C-termini, respectively. For pH 7 we used the 2+ pattern [$nt^{+}R^{+}PPGFSPFR^{+}ct^{-}$], while for pH 10 the peptide charge was 1+ [$nt^{0}R^{+}PPGFSPFR^{+}ct^{-}$].

Results and Discussion

ESI-MS Experiments. Mass spectra of bradykinin electrosprayed in aqueous solutions at pH values of 2, 7, and 10 are shown in Figure 1. Consistent with earlier results,[53, 61, 68-72] the spectra showed charge states of 3+ down to 1+. The pH 2 data were dominated by 3+ ions (av. charge 2.7+, Figure 1A). At pH 10, the most intense charge state was 2+ (av. charge 2.1+, Figure 1C). These observations demonstrate that bulk solution pH has a certain effect on the ESI charge state distribution of bradykinin. However, the observed pH dependence is less pronounced than one might expect from the peptide charge in solution (which shifts from 3+ at pH 2 to 1+ at pH 10, Figure S1). The observed behavior is consistent with earlier experiments, which demonstrated that there tends to be a disparity between peptide charge in solution and in the gas phase, although some trends persist (i.e., somewhat higher ESI charge states at acidic pH).[61]

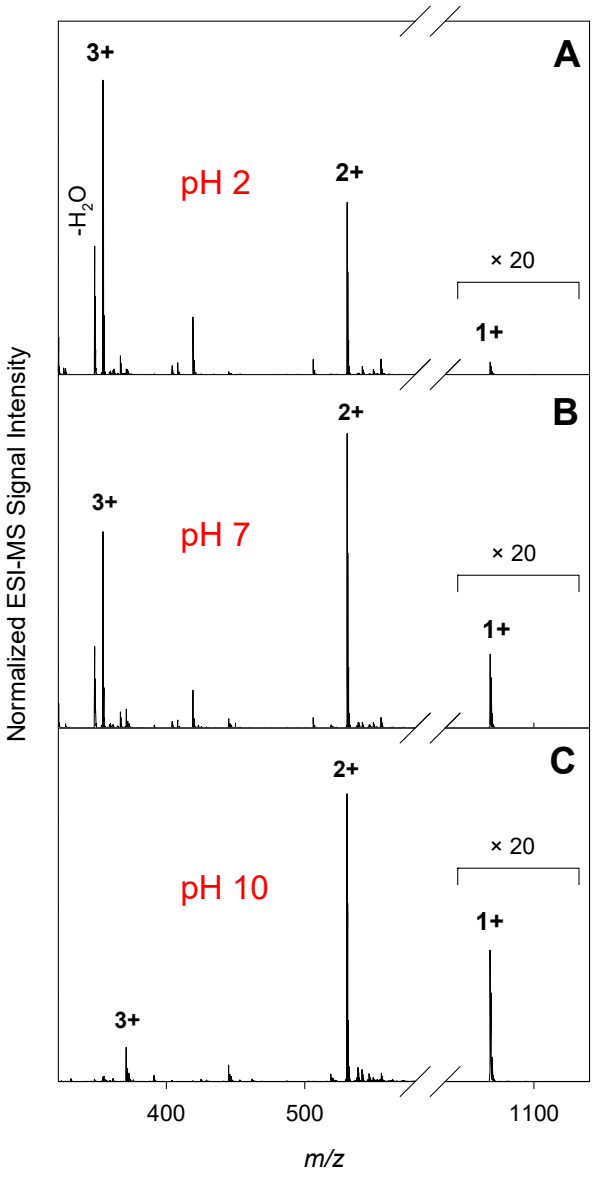

Figure 1. ESI mass spectra of bradykinin acquired in aqueous solution at (A) pH 2, (B) pH 7, and (C) pH 10. The charge states z of the $[M + zH]^{z+}$ ions are indicated. The signal intensity of the 1+ region has been magnified by a factor of twenty in all three panels. The $-H_2O$ signal seen for 3+ bradykinin is consistent with data on other Ser-containing peptides,[94] reflecting the fact that the 3+ ions experience more collisional activation during ion sampling than the 2+ and 1+ species.

The peptide ions in the spectra of Figure 1 had a $[M + zH]^{z+}$ composition. We repeated the experiments in the presence of 0.5 mM NaCl, generating ions that were charged by a combination of protonation and sodiation ($[M + (z\text{-}i)H + iNa]^{z+}$, Figure S2). ESI charge states seen for those

NaCl-containing solutions were similar to those of Figure 1, revealing that the outcome of the ESI process is largely independent of the charge carrier used (H^+ or Na^+). This is important when comparing experiments and MD results, keeping in mind that our simulations employed droplets charged with Na^+.[24, 26, 45, 54, 55]

ESI Simulations on Bradykinin at pH 2. The primary focus of our MD simulations was on the ESI behavior of bradykinin in acidic solution, because most peptide ESI analyses are conducted at low pH.[7-10] Conveniently, changes in droplet acidity during evaporation are not an issue under these conditions, rendering pH 2 simulations conceptually straightforward (see Methods). MD runs were conducted by embedding 3+ bradykinin in Rayleigh-charged water droplets. Like in earlier simulations on other analytes,[24, 26] the MD runs showed rapid water evaporation. Occasional IEM ejection of Na^+ kept the shrinking droplets close to the Rayleigh limit. This water and Na^+ behavior has been discussed in detail elsewhere.[26, 43-45, 47]

Figure 2A exemplifies snapshots from an MD run on an ESI droplet with an initial radius r_0 = 4 nm. The 13.5 ns time point illustrates a Na^+ ejection event. Also at this time, bradykinin had moved close to the droplet surface. However, in this trajectory the peptide remained within the droplet until the solvent had completely evaporated at $t \approx 75$ ns. In other words, formation of the $[M + 3H]^{3+}$ peptide ion in Figure 2A followed the CRM. Similar CRM trajectories have previously been reported in MD studies on other 3+ peptides.[49, 53, 66]

Figure 2B shows MD data for a droplet with r_0 = 5 nm. Once again, the droplet underwent water evaporation with IEM ejection of Na^+ (t = 2.25 ns in Figure 2B). Unlike in the aforementioned CRM run, bradykinin was ejected from the droplet at $t \approx 3.24$ ns. The departing peptide left behind an analyte-free residual droplet. Immediately after ejection, the peptide remained bound to ca. 50 water molecules which then evaporated, ultimately generating a $[M + 3H]^{3+}$ gaseous ion (Figure 2B,

t = 75 ns). Ejection of bradykinin from the droplet in Figure 2B signifies the hallmark of the IEM. To our knowledge, this is the first time that droplet MD simulations confirmed the viability of gaseous peptide ion formation via the IEM. More generally, Figure 2 demonstrates that both the IEM and the CRM can produce gaseous bradykinin ions.

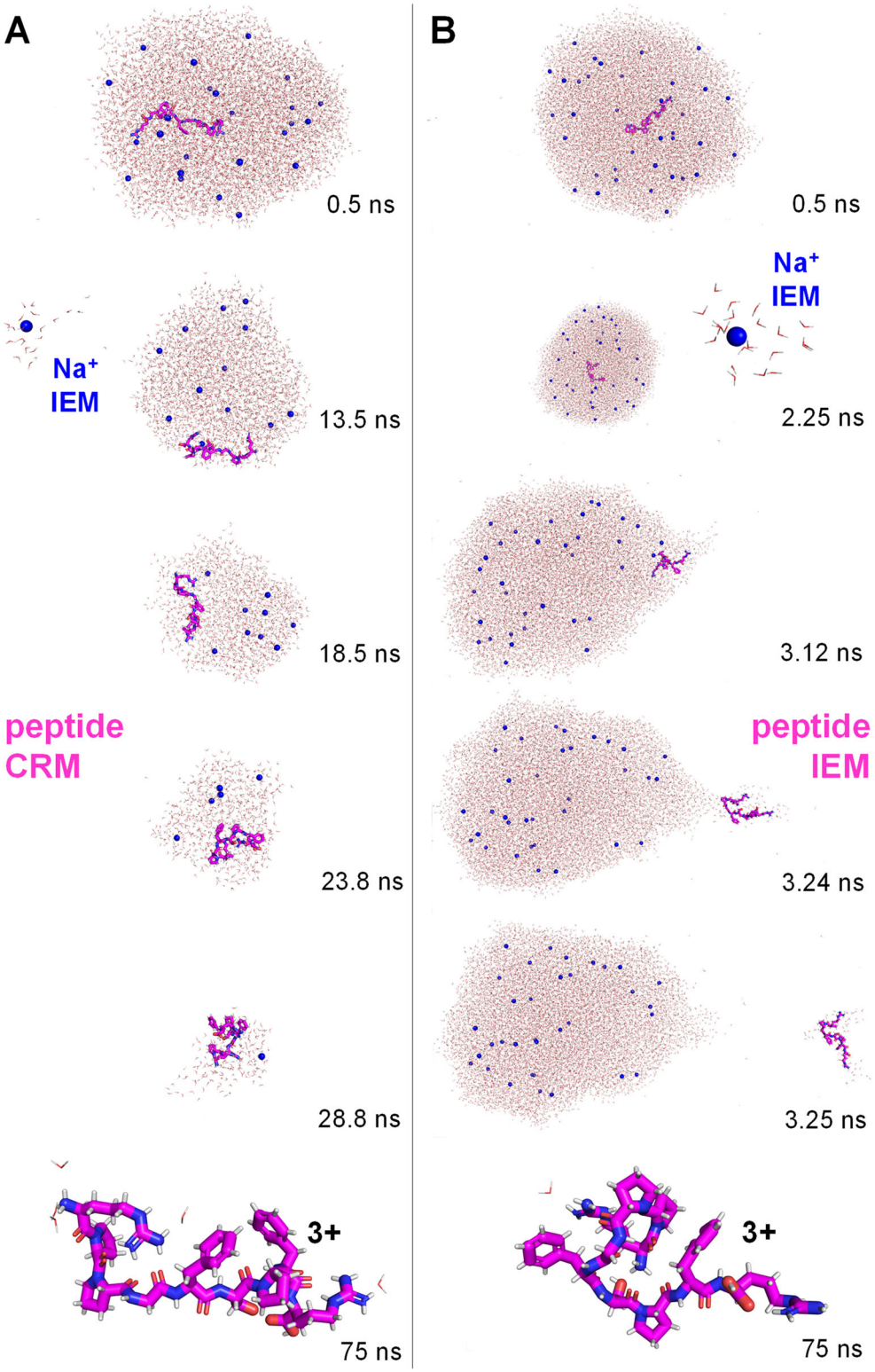

Figure 2. MD trajectory snapshots of aqueous ESI droplets containing 3+ bradykinin (pink) and excess Na^+ (blue) for various time points, representing a pH 2 droplet. (A) Initial droplet radius r_0 = 4 nm, culminating in $[M + 3H]^{3+}$ ion formation via the CRM. (B) r_0 = 5 nm, with $[M + 3H]^{3+}$ ion formation via the IEM. Both trajectories also show IEM ejection of Na^+, highlighted in blue.

Multiple pH 2 simulations were conducted to examine which factor(s) govern the prevalence of IEM vs. CRM behavior. MD runs for initial droplet radii between 1.5 nm and 5 nm all produced $[M + 3H]^{3+}$ gaseous ions. A quick way to recognize the ESI mechanism in the MD data is to track the number of water molecules surrounding the peptide. All of the profiles in Figure 3 start off with a gradual decrease that reflects water evaporation from the droplet. For CRM trajectories, this decrease continued all the way to zero, implying that the peptide was released by solvent evaporation to dryness. Conversely, IEM trajectories exhibited near-vertical transitions at the point of peptide ejection. Almost all of the MD runs on droplets with r_0 between 5.0 nm and 4.0 nm culminated in IEM ejection of bradykinin. Droplets with r_0 = 3.5 nm and 3.0 nm resulted in a mix, where some peptides showed IEM behavior while others followed the CRM (Figure 3A). The smallest droplets (r_0 = 2.0 nm and 1.5 nm, Figure 3B) exclusively showed CRM behavior. This trend is also apparent from Figure 4A, which shows the percentage of each ESI mechanism for all r_0 values. Before discussing the origin of this trend, we will have a look at additional simulation results.

ESI Simulations at pH 7 and pH 10. MD runs for pH 7 were conducted by adjusting the solution charge of bradykinin to 2+ (Figure S1). Most of these simulations produced gaseous peptide ions via the CRM (Figure S3A). Only some runs showed IEM behavior (Figure S3B). The majority of the pH 7 simulations culminated in $[M + 2H]^{2+}$ gaseous ions. The remaining runs involved attachment of one Na^+, generating $[M + 2H + 1Na]^{3+}$ ions. Na^+ binding to bradykinin involved electron-rich moieties, such as backbone carbonyl oxygens and the C-terminal carboxylate (Figure S3, t = 75 ns). This occasional sodiation took place for both IEM and for CRM runs. The CRM vs. IEM balance, as well as the final charge states of all pH 7 simulations are compiled in Figure 4B.

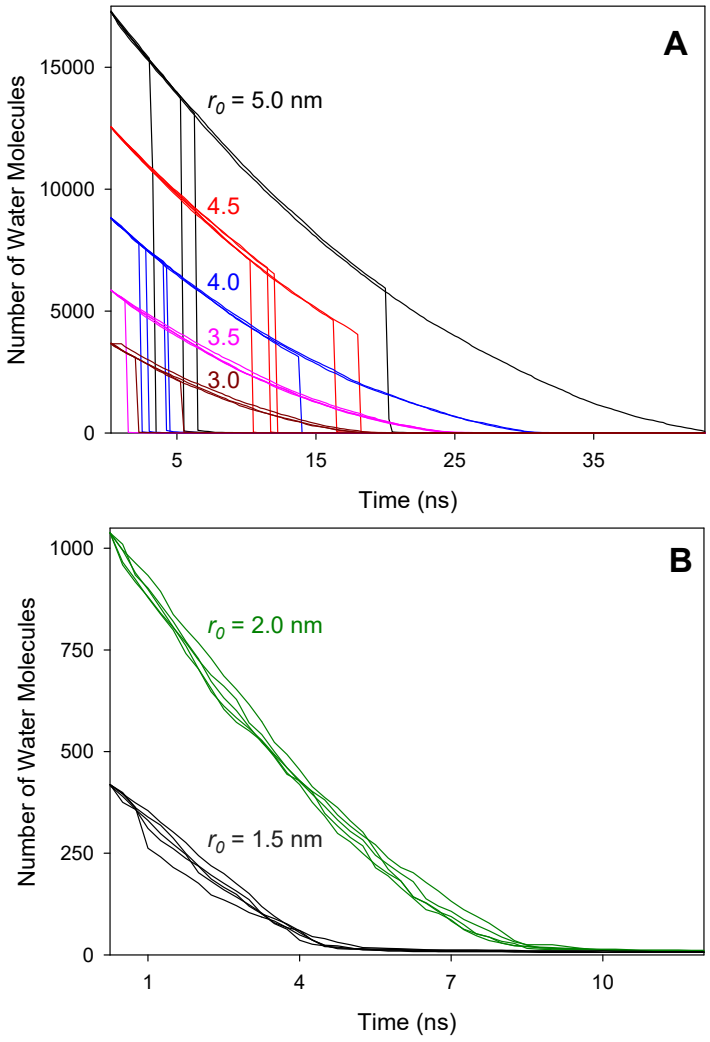

Figure 3. ESI simulation results from multiple MD runs on bradykinin in droplets with different initial radius r_0. (A) r_0 = 5.0 nm to 3.0 nm, (B) r_0 = 2.0 nm and 1.5 nm. The simulations mimic pH 2 droplets with a 3+ peptide charge in solution. All runs generated $[M + 3H]^{3+}$ gaseous ions. Graphs display the number of water molecules surrounding the peptide. Sudden downward transitions indicate IEM ejection of the peptide. CRM runs are characterized by a gradual decrease toward zero as droplets evaporate to dryness. The profiles shown here represent five to seven independent MD runs for each droplet radius.

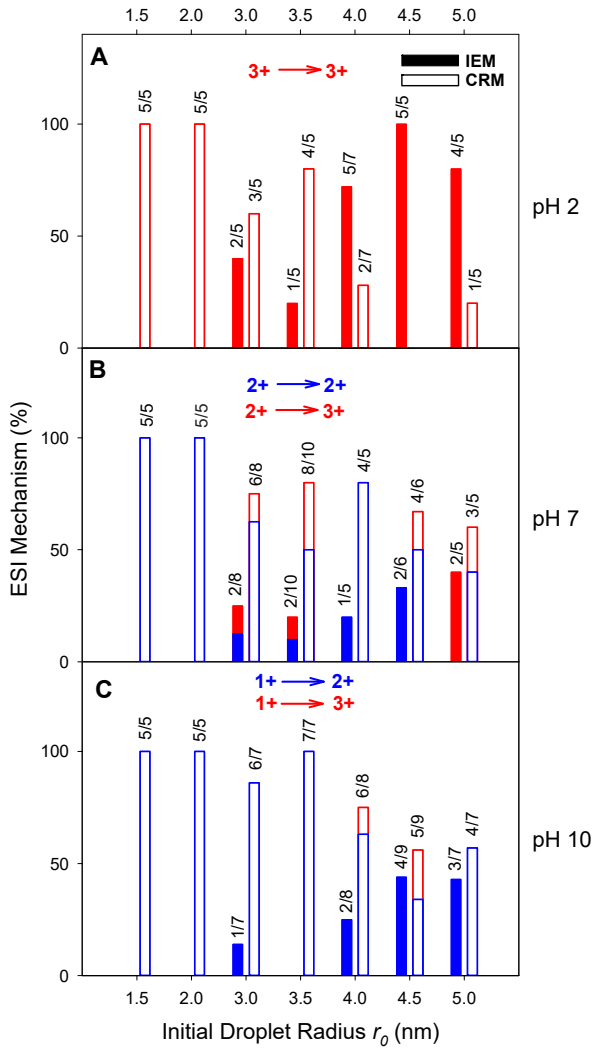

Figure 4. Summary of MD simulation results for bradykinin in differently sized droplets. Gaseous peptide ions were formed via the IEM (filled bars) or the CRM (open bars). The initial bradykinin charge in solution was (A) 3+, corresponding to pH 2; (B) 2+, corresponding to pH 7; (C) 1+, corresponding to pH 10. The percentage of each ESI mechanism is shown on the y-axis. Different colors in each panel distinguish final charge states. The *i*/*j* notation indicates the number of runs that showed a specific mechanism (*i*) for the total number of runs under that condition (*j*).

At pH 10 the solution charge of bradykinin is 1+ (Figure S1), but none of these simulations produced a singly charged gaseous peptide. Instead, all runs involved binding of one or two Na^+, generating $[M + 1H + 1Na]^{2+}$ or $[M + 1H + 2Na]^{3+}$ ions. Most of these gaseous peptides were formed

via the CRM. IEM behavior was seen in some runs for larger droplets, but never for $r_0 < 3$ nm (Figure 4C). Evaporation kinetics at pH 7 and pH 10 are shown in Figures S4 and S5.

Comparing MD Data and Experiments. The pH-dependent simulation results are in good agreement with our experimental ESI-MS data. Changing the pH from 2 to 7 to 10 caused a 2.7+ → 2.5+ → 2.1+ shift in the average charge state of the experimental mass spectra (Figure 1). The average MD charge states showed a similar shift (3.0+ → 2.2+ → 2.1+, Figure 4). Simulated bradykinin ions exclusively appeared as 3+ and 2+ ions, matching the dominant charge states in the experiments. This agreement is not trivial because, in principle, Na^+ binding could have generated charge states $z > 3$ during the MD runs, but neither the simulations nor the experiments showed such highly charged ions. Similarly, pH 10 simulations could have produced 1+ gaseous ions. Instead all of the corresponding MD runs produced 2+ or 3+ charge states, consistent with experiments of Figure 1C where the 1+ contribution was very low (about 1%). The overall agreement between MD results and experiments supports the validity of the modeling strategy used here.

Proteins comprise a much larger number of residues compared to peptides. For those large molecules, lowering the bulk pH often causes dramatic shifts to higher ESI charge states as a result of unfolding in solution.[26, 95-97] In comparison, the pH dependent shifts seen for bradykinin (Figure 1) and similar peptides[61] are more moderate. Still, the question arises if these peptide shifts are also related to unfolding. Our data indicate that this is not the case. Bradykinin can adopt transient structure in solution,[69] but its overall conformation is disordered[85] This disorder is consistent with the near-instantaneous deuteration of bradykinin.[98] The formation of stable secondary structure is hindered by the large percentage of Pro (3/9 residues).[99] The inability of bradykinin to adopt a folded state in solution precludes the occurrence of unfolding. This view is supported by MD data for bradykinin in droplets between pH 2 and 10, all of which showed disordered conformations as

exemplified in Figure S6 (although collapse into more compact structures can take place after release into the gas phase, particularly for 1+ ions[72]). We conclude that pH-dependent ESI charge state shifts of bradykinin are not caused by unfolding in solution. Instead, these shifts appear to be a remnant of the peptide protonation pattern in solution, although there is no 1:1 correlation between analyte charge before and after ESI.[61-63]

It is interesting that at pH 2 the solution charge of bradykinin is 3+ (Figure S1), while the corresponding experimental spectrum showed ~30% 2+ ions (Figure 1A). We tentatively attribute these 2+ ions to charge loss during IEM ejection, when some of the departing peptides leave one proton behind in the droplet. Similar events can take place for proteins during the CEM.[26] Our MD strategy did not allow for such H^+ transfer. Instead, all of our pH 2 simulations culminated in $[M + 3H]^{3+}$ ions, matching the dominant (~70%) signal in the experimental spectrum of Figure 1A.

Previous work suggested that natively folded proteins predominantly follow the CRM.[11, 25, 26, 39] The ESI charge states z of these CRM-generated ions approximately match z_R of protein-sized water droplets, as expected if the net charge of the shrinking ESI droplets stays close to the Rayleigh limit (eq. 1).[11, 19] This $z \approx z_R$ relationship also holds for the CRM-generated peptide ions examined here. When using a density of 1 g cm^{-3}, bradykinin (1060 Da) has an effective radius of 0.75 nm.[19] From this radius eq. 1 predicts z = 2.3+, which is within the range observed in our experiments and simulations (Figures 1, 4). However, this agreement does not provide clues to the ESI mechanism, because CRM and IEM simulations both generated the same charge state range (Figure 4).

Competition Between ESI Mechanisms. Our MD data reveal that IEM and CRM are both viable for the formation of gaseous peptide ions. The distinction between the two mechanisms was clear-cut; there was no "intermediate" ESI scenario under the conditions of this work. Figure 4 implies that the prevalence of IEM ejection follows two trends. (1) Peptide charge in solution (q_{pep}) is a key

factor. IEM behavior was much more common for q_{pep} = 3+ than for q_{pep} = 2+. Peptides with q_{pep} = 1+ were incapable of IEM ejection, unless Na^+ binding generated a 2+ ion. (2) The other key factor is the initial droplet radius r_0. IEM ejection was favored for larger droplets (r_0 = 4 nm to 5 nm), while none of the runs for r_0 < 3 nm showed IEM behavior.

A simple model can qualitatively account for the dependence of IEM ejection on q_{pep} and r_0 (Figure 5). IEM events are driven by the repulsive force F between q_{pep} and the droplet charge $q_{drop} = q_R - q_{pep}$.[21-24] Droplet and peptide are approximated as spheres, with r_{pep} = 0.75 nm as noted earlier. We focus on a situation where the peptide is poised to undergo IEM ejection and has moved to the outside surface of the droplet (right hand side in Figure 5A,B). One can calculate the dependence of F on q_{pep} and r_0 by noting that $F = E \times q_{pep}$, with the electric field $E = (4\pi\varepsilon_0)^{-1}\, q_{drop} / (r_{drop} + r_{pep})^2$.

The magnitude of F governs the IEM vs. CRM competition. If F is small, the peptide will be pulled back into the droplet as a result of solvent polarization, image charges, and surface tension effects.[21, 22] Our model does not explicitly consider these opposing factors. Instead, we focus on the premise that a large F will favor separation of peptide and droplet, thereby promoting IEM behavior. Figure 5A illustrates the situation for r_0 = 1.5 nm and q_{pep} = 3+, with F = 0.52 nN. Increasing the droplet size to r_0 = 4.5 nm boosts F to 0.78 nN, Figure 5B). It is obvious that this larger repulsion will promote IEM ejection in Figure 5B. Peptide/droplet separation is less likely in Figure 5A, favoring retention of the peptide in the droplet until the solvent has evaporated to dryness (CRM).

$F(r_0)$ plots for different q_{pep} show that 3+ peptides experience the highest repulsive force, while F is lowest for q_{pep} = 1+ (Figure 5C). This predicted dependence accounts for Trend (1) identified above; i.e., the fact that a high peptide charge solution (caused by low pH) favors IEM ejection. The maximum of the $F(r_0)$ plot for q_{pep} = 3+ is at r_0 = 4 nm (Figure 5C). Thus, our model predicts that IEM ejection will be most favorable for droplets in this size range. Smaller droplets will preferentially exhibit CRM behavior. This prediction accounts for Trend (2), i.e. the low

prevalence of IEM events for very small droplets. One can explain the second trend by noting that for very small r_0, a significant fraction of overall charge (q_R) is contributed by q_{pep}. Under these conditions, the remaining q_{drop} is so small that only a relatively weak repulsive force F is generated (Figure 5A). F is more favorable for larger droplets (e.g. $r_0 = 4.5$ nm, Figure 5B), where IEM ejection becomes more likely. Much larger droplets once again show lower F values, because $E \propto r_0^{-1/2}$ for Rayleigh-charged droplets with $r_{pep} << r_{drop}$ and $q_{pep} << q_{drop}$.[22, 24, 100] Although the low E of very large droplets prevents peptide IEM, these droplets may shrink until they reach a size regime where F is adequate for peptide ejection (e.g., from $r_0 = 50$ nm to 4 nm along the red profile in Figure 5C). However, fission events cause discontinuous size changes, such that not all droplets will necessarily pass through the regime where IEM is favored. Unfortunately, computational cost precludes MD simulations on such very large droplets.

The approximate minimum force F_{min} required for peptide IEM is indicated by the dashed line in Figure 5C. F_{min} was estimated by noting that IEM events become feasible for 2+ (pH 7) bradykinin in the r_0 range between 3 nm to 5 nm (Figure 4B). Conditions where $F > F_{min}$ allow for peptide IEM ejection. Conditions below this threshold favor peptide ion formation via the CRM, unless the droplet is very large and can shrink until $F > F_{min}$. It is gratifying that our model can account for the trends of IEM ejection on q_{pep} and r_0 that were seen in the MD simulations. However, we emphasize the minimalist nature of this model which neglects many aspects of droplet behavior.

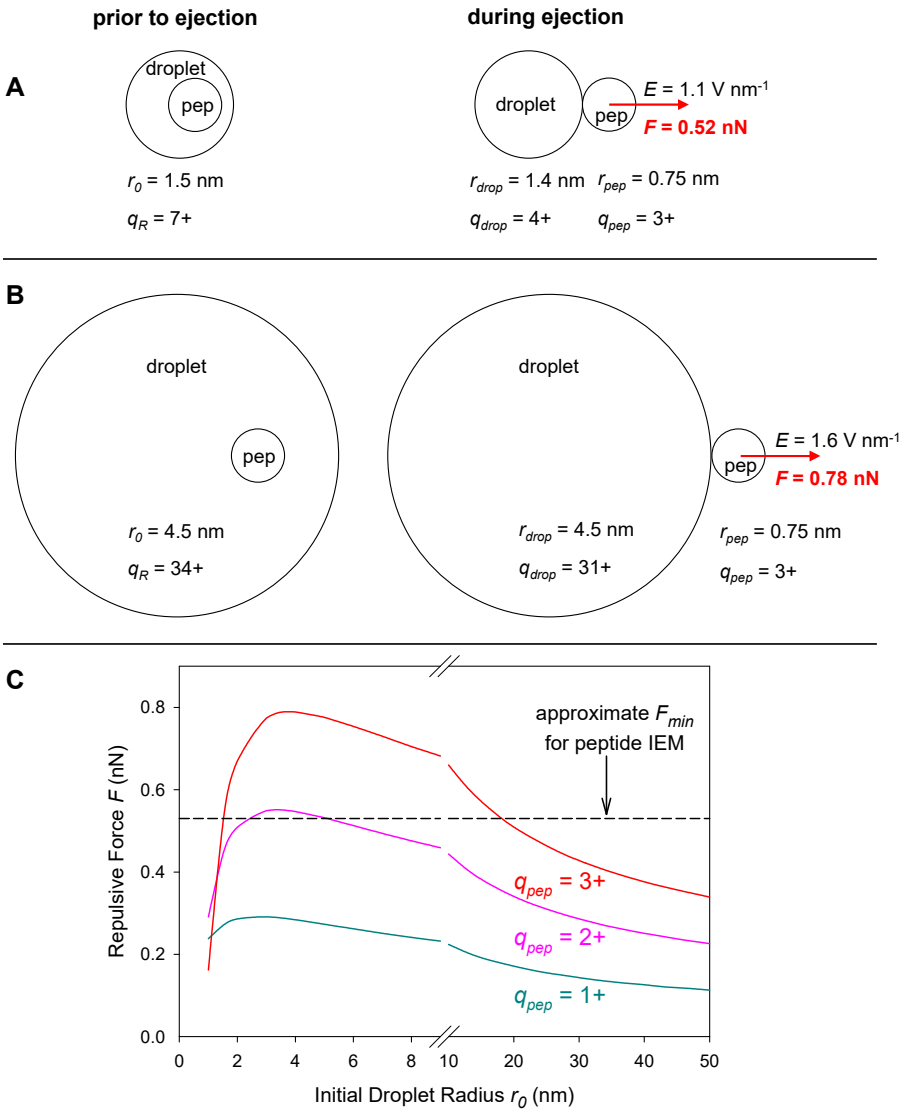

Figure 5. Simple electrostatic model to calculate the force F acting on a peptide ion ("pep") during IEM ejection. Droplet and peptide are modeled as charged spheres. (A) The left cartoon shows a droplet with r_0 = 1.5 nm at the Rayleigh limit prior to ejection. The cartoon on the right shows the peptide during ejection. The repulsive force F acting on the peptide at this point is indicated in red. (B) Same as in panel A, but for a droplet with r_0 = 4.5 nm. (C) Dependence of F on r_0 for different values of q_{pep}. For additional details, see text.

Conclusions

How are gaseous peptide ions formed during the ESI process? The current work reveals that the answer to this question is not straightforward. Using bradykinin under acidic conditions (solution

charge 3+) as a model peptide, both the IEM and the CRM were found to be viable. Droplets with radii between 4 and 5 nm showed mostly IEM behavior, whereas for smaller droplets the CRM was dominant. Our data resolve a conundrum in the literature; on the one hand it is widely believed that peptides follow the IEM,[13, 36, 64, 65] while on the other hand earlier simulations showed peptide CRM behavior.[49, 53, 66] Notably, those earlier simulations used relatively small droplets ($r_0 \approx 3$ nm). Our data confirm that the CRM is dominant for droplets in this size range, whereas IEM behavior becomes prevalent for droplets that are somewhat larger (Figure 4).

Even after verifying that peptide ions can form through both mechanisms, it remains difficult to predict the IEM vs. CRM balance under experimental conditions. This is because the ESI plume comprises a wide droplet size range (particularly with the high flow rates used for LC/MS), covering radii of ~ 1 μm down to 2 nm and below.[11, 18] If solvent evaporation were the only shrinkage process, all of the early (large) ESI droplets would automatically pass through the 4-5 nm regime where IEM is favorable. However, in reality Coulomb fission plays a dominant role as well,[11, 18] such that droplets may "skip over" this IEM regime. For example, formation of 2 nm progeny droplets from a 10 nm parent droplet will miss the 4-5 nm range where IEM ejection is likely to happen. In other words, before predicting the prevalent peptide ESI mechanism under experimental conditions, it will be necessary to obtain a better understanding of the droplet size distribution in the ESI plume. The results of the current work specifically apply to bradykinin. It is to be expected that the IEM vs. CRM balance will also be affected by the amino acid composition, including the percentage of nonpolar side chains and the number of titratable sites.[54] Efforts to tackle these issues are currently underway in our laboratory, and the results will be reported elsewhere.

Supporting Information. Figure S1: Titration profile of bradykinin in solution. Figure S2: Bradykinin mass spectra acquired in the presence of NaCl. Figure S3: MD trajectory snapshots for

bradykinin with an initial 2+ charge. Figure S4: MD-generated evaporation profiles for bradykinin with an initial 2+ charge. Figure S5: MD-generated evaporation profiles for bradykinin with an initial 1+ charge. Figure S6: MD conformations of bradykinin at different pH.

References

(1) Fenn, J. B. Electrospray Wings for Molecular Elephants (Nobel Lecture). *Angew. Chem. Int. Ed.* **2003**, 42, 3871-3894.

(2) Leney, A. C.; Heck, A. J. R. Native Mass Spectrometry: What is in the Name? *J. Am. Soc. Mass Spectrom.* **2017**, 28, 5-13.

(3) Mehmood, S.; Allison, T. M.; Robinson, C. V. Mass Spectrometry of Protein Complexes: From Origins to Applications. *Annu. Rev. Phys. Chem.* **2015**, 66, 453-474.

(4) Donnelly, D. P.; Rawlins, C. M.; DeHart, C. J.; Fornelli, L.; Schachner, L. F.; Lin, Z. Q.; Lippens, J. L.; Aluri, K. C.; Sarin, R.; Chen, B. F.; Lantz, C.; Jung, W.; Johnson, K. R., et al. Best practices and benchmarks for intact protein analysis for top-down mass spectrometry. *Nat. Methods* **2019**, 16, 587-594.

(5) Zhang, Y.; Fonslow, B. R.; Shan, B.; Baek, M.-C.; Yates, J. R. Protein Analysis by Shotgun/Bottom-up Proteomics. *Chem. Rev.* **2013**, 113, 2343-2394.

(6) Aebersold, R.; Mann, M. Mass spectrometry-based proteomics. *Nature* **2003**, 422, 198-207.

(7) Gussakovsky, D.; Anderson, G.; Spicer, V.; Krokhin, O. V. Peptide separation selectivity in proteomics LC-MS experiments: Comparison of formic and mixed formic/heptafluorobutyric acids ion-pairing modifiers. *J. Sep. Sci.* **2020**, 43, 3830-3839.

(8) Olsen, J. V.; Ong, S.; Mann, M. Trypsin Cleaves Exlusively C-terminal to Arginine and Lysine Residues. *Mol. Cell. Proteomics* **2004**, 3, 608-614.

(9) Zhu, W. H.; Venable, J.; Giometti, C. S.; Khare, T.; Tollaksen, S.; Ahrendt, A. J.; Yates, J. R. Large-scale mu LC-MS/MS for silver- and Coomassie blue-stained polyacrylamide gels. *Electrophoresis* **2005**, 26, 4495-4507.

(10) Huang, Y.; Triscari, J. M.; Tseng, G. C.; Pasa-Tolic, L.; Lipton, M. S.; Smith, R. D.; Wysocki, V. H. Statistical characterization of the charge state and residue dependence of low-energy CID peptide dissociation patterns. *Anal. Chem.* **2005**, 77, 5800-5813.

(11) Kebarle, P.; Verkerk, U. H. Electrospray: From Ions in Solutions to Ions in the Gas Phase, What We Know Now. *Mass Spectrom. Rev.* **2009**, 28, 898-917.

(12) Cech, N. B.; Enke, C. G. Practical Implication of Some Recent Studies in Electrospray Ionization Fundamentals. *Mass Spectrom. Rev.* **2001**, 20, 362-387.

(13) Thomson, B. A. Atmospheric Pressure Ionization and Liquid Chromatography/Mass Spectrometry-Together at Last. *J. Am. Soc. Mass Spectrom.* **1998**, 9, 187-193.

(14) Szarka, M.; Szigeti, M.; Guttman, A. Imaging Laser-Induced Fluorescence Detection at the Taylor Cone of Electrospray Ionization Mass Spectrometry. *Anal. Chem.* **2019**, 91, 7738-7743.

(15) Gibson, G. T. T.; Mugo, S. M.; Oleschuk, R. D. Nanoelectrospray Emitters: Trends and Perspective. *Mass Spectrom. Rev.* **2009**, 28, 918-936.

(16) Wilm, M. S.; Mann, M. Electrospray and Taylor-Cone theory, Dole's beam of macromolecules at last? *Int. J. Mass Spectrom.* **1994**, 136, 167-180.

(17) Nemes, P.; Marginean, I.; Vertes, A. Spraying Mode Effect on Droplet Formation and Ion Chemistry in Electrosprays. *Anal. Chem.* **2007**, 79, 3105-3116.

(18) Grimm, R. L.; Beauchamp, J. L. Evaporation and Discharge Dynamics of Highly Charged Multicomponent Droplets Generated by Electrospray Ionization. *J. Phys. Chem. A* **2010**, 114, 1411-1419.

(19) de la Mora, J. F. Electrospray Ionization of large multiply charged species proceeds via Dole's charged residue mechanism. *Anal. Chim. Acta* **2000**, 406, 93-104.

(20) Harper, C. C.; Brauer, D. D.; Francis, M. B.; Williams, E. R. Direct observation of ion emission from charged aqueous nanodrops: effects on gaseous macromolecular charging. *Chem. Sci.* **2021**, 12, 5185-5195.
(21) Iribarne, J. V.; Thomson, B. A. On the evaporation of small ions from charged droplets. *J. Chem. Phys.* **1976**, 64, 2287-2294.
(22) Loscertales, I. G.; de la Mora, J. F. Experiments on the kinetics of field evaporation of small ions from droplets. *J. Chem. Phys.* **1995**, 103, 5041-5060.
(23) McQuinn, K.; Hof, F.; McIndoe, J. S. Direct observation of ion evaporation from a triply charged nanodroplet. *Chem. Commun.* **2007**, 2007, 4099-4101.
(24) Aliyari, E.; Konermann, L. Formation of Gaseous Proteins via the Ion Evaporation Model (IEM) in Electrospray Mass Spectrometry. *Anal. Chem.* **2020**, 92, 10807-10814.
(25) Dole, M.; Mack, L. L.; Hines, R. L.; Mobley, R. C.; Ferguson, L. D.; Alice, M. B. Molecular beams of macroions. *J. Chem. Phys.* **1968**, 49, 2240-2249.
(26) Konermann, L.; Metwally, H.; Duez, Q.; Peters, I. Charging and Supercharging of Proteins for Mass Spectrometry: Recent Insights into the Mechanisms of Electrospray Ionization. *Analyst* **2019**, 144, 6157-6171.
(27) Consta, S.; Chung, J. K. Charge-Induced Conformational Changes of PEG-(Na+)n in Vacuum and Aqueous Nanodroplets. *J. Phys. Chem. B* **2011**, 115, 10447-10455.
(28) Donor, M. T.; Ewing, S. A.; Zenaidee, M. A.; Donald, W. A.; Prell, J. S. Extended Protein Ions Are Formed by the Chain Ejection Model in Chemical Supercharging Electrospray Ionization. *Anal. Chem.* **2017**, 89, 5107-5114.
(29) Cole, R. B. Some tenets pertaining to electrospray ionization mass spectrometry. *J. Mass. Spectrom.* **2000**, 35, 763-772.
(30) Beveridge, R.; Phillips, A. S.; Denbigh, L.; Saleem, H. M.; MacPhee, C. E.; Barran, P. E. Relating gas phase to solution conformations: Lessons from disordered proteins. *Proteomics* **2015**, 15, 2872-2883.
(31) Hogan, C. J.; Carroll, J. A.; Rohrs, H. W.; Biswas, P.; Gross, M. L. Combined Charged Residue-Field Emission Model of Macromolecular Electrospray Ionization. *Anal. Chem.* **2009**, 81, 369-377.
(32) Ogorzalek Loo, R. R.; Lakshmanan, R.; Loo, J. A. What Protein Charging (and Supercharging) Reveal about the Mechanism of Electrospray Ionization. *J. Am. Soc. Mass Spectrom.* **2014**, 25, 1675-1693.
(33) Marchese, R.; Grandori, R.; Carloni, R.; Raugei, S. A Computational Model for Protein Ionization by Electrospray Based on Gas-Phase Basicity. *J. Am. Soc. Mass Spectrom.* **2012**, 23, 1903-1910.
(34) Hamdy, O. M.; Julian, R. R. Reflections on Charge State Distributions, Protein Structure, and the Mystical Mechanism of Electrospray Ionization. *J. Am. Soc. Mass Spectrom.* **2012**, 23, 1-6.
(35) Wang, G.; Cole, R. B. Charged residue versus ion evaporation for formation of alkali metal halide clusters ions in ESI. *Anal. Chim. Acta* **2000**, 406, 53-65.
(36) Nguyen, S.; Fenn, J. B. Gas-phase ions of solute species from charged droplets of solutions. *Proc. Natl. Acad. Sci. U.S.A.* **2007**, 104, 1111-1117.
(37) Spencer, E. A. C.; Ly, T.; Julian, R. K. Formation of the serine octamer: Ion evaporation or charge residue? *Int. J. Mass Spectrom.* **2008**, 270, 166-172.
(38) Siu, K. W. M.; Guevremont, R.; Le Blanc, J. C. Y.; O'Brien, R. T.; Berman, S. S. Is Droplet Evaporation Crucial in the Mechanism of Electrospray Mass Spectrometry? *Org. Mass Spectrom.* **1993**, 28, 579-584.

(39) Iavarone, A. T.; Williams, E. R. Mechanism of Charging and Supercharging Molecules in Electrospray Ionization. *J. Am. Chem. Soc.* **2003**, 125, 2319-2327.
(40) Liuni, P.; Wilson, D. J. Understanding and optimizing electrospray ionization techniques for proteomic analysis. *Exp. Rev. Proteomics* **2011**, 8, 197-209.
(41) Wilm, M. Principles of Electrospray Ionization. *Mol. Cell. Proteomics* **2011**, 10, 0094071-0094078.
(42) Fenn, J. B. Ion Formation from Charged Droplets: Roles of Geometry, Energy, and Time. *J. Am. Soc. Mass Spectrom.* **1993**, 4, 524-535.
(43) Znamenskiy, V.; Marginean, I.; Vertes, A. Solvated Ion Evaporation from Charged Water Droplets. *J. Phys. Chem. A* **2003**, 107, 7406-7412.
(44) Ichiki, K.; Consta, S. Disintegration Mechanisms of Charged Aqueous Nanodroplets Studied by Simulations and Analytical Models. *J. Phys. Chem. B* **2006**, 110, 19168-19175.
(45) Caleman, C.; van der Spoel, D. Evaporation from water clusters containing singly charged ions. *Phys. Chem. Chem. Phys.* **2007**, 9, 5105-5111.
(46) Steinberg, M. Z.; Breuker, K.; Elber, R.; Gerber, R. B. The dynamics of water evaporation from partially solvated cytochrome c in the gas phase. *Phys. Chem. Chem. Phys.* **2007**, 9, 4690-4697.
(47) Luedtke, W. D.; Landmann, U.; Chiu, Y.-H.; Levandier, D. J.; Dressler, R. A.; Sok, S.; Gordon, M. S. Nanojets, Electrospray and Ion Field Evaporation: Molecular Dynamics Simulations and Laboratory Experiments. *J. Phys. Chem. A* **2008**, 112, 9628-9649.
(48) Higashi, H.; Tokumi, T.; Hogan, C. J.; Suda, H.; Seto, T.; Otani, Y. Simultaneous ion and neutral evaporation in aqueous nanodrops: experiment, theory, and molecular dynamics simulations. *Phys. Chem. Chem. Phys.* **2015**, 17, 15746-15755.
(49) Kim, D.; Wagner, N.; Wooding, K.; Clemmer, D. E.; Russell, D. H. Ions from Solution to the Gas Phase: A Molecular Dynamics Simulation of the Structural Evolution of Substance P during Desolvation of Charged Nanodroplets Generated by Electrospray Ionization. *J. Am. Chem. Soc.* **2017**, 139, 2981-2988.
(50) Porrini, M.; Rosu, F.; Rabin, C.; Darre, L.; Gomez, H.; Orozco, M.; Gabelica, V. Compaction of Duplex Nucleic Acids upon Native Electrospray Mass Spectrometry. *ACS Central Sci.* **2017**, 3, 454–461.
(51) Kondalaji, S. G.; Khakinejad, M.; Valentine, S. J. Comprehensive Peptide Ion Structure Studies Using Ion Mobility Techniques: Part 3. Relating Solution-Phase to Gas-Phase Structures. *J. Am. Soc. Mass Spectrom.* **2018**, 29, 1665-1677.
(52) Beveridge, R.; Migas, L. G.; Das, R. K.; Pappu, R. V.; Kriwacki, R. W.; Barran, P. E. Ion Mobility Mass Spectrometry Uncovers the Impact of the Patterning of Oppositely Charged Residues on the Conformational Distributions of Intrinsically Disordered Proteins. *J. Am. Chem. Soc.* **2019**, 141, 4908-4918.
(53) Aschi, M. From the solution to the gas phase: A numerical experiment on the electrospray process of triprotonated Bradykinin. *Int. J. Mass Spectrom.* **2019**, 438, 44-54.
(54) Calixte, E. I.; Liyanage, O. T.; Kim, H. J.; Ziperman, E. D.; Pearson, A. J.; Gallagher, E. S. Release of Carbohydrate-Metal Adducts from Electrospray Droplets: Insight into Glycan Ionization by Electrospray. *J. Phys. Chem. B* **2020**, 124, 479-486.
(55) Luan, M. J.; Hou, Z. H.; Huang, G. M. Suppression of Protein Structural Perturbations in Native Electrospray Ionization during the Final Evaporation Stages Revealed by Molecular Dynamics Simulations. *J. Phys. Chem. B* **2022**, 126, 144−150.
(56) Rodriguez, J.; Gupta, N.; Smith, R. D.; Pevzner, P. A. Does Trypsin Cut Before Proline? *J. Proteome Res.* **2008**, 7, 300-305.

(57) Tsiatsiani, L.; Heck, A. J. R. Proteomics beyond trypsin. *FEBS J.* **2015**, 282, 2612-2626.
(58) Swaney, D. L.; Wenger, C. D.; Coon, J. J. Value of Using Multiple Proteases for Large-Scale Mass Spectrometry-Based Proteomics. *J. Proteome Res.* **2010**, 9, 1323-1329.
(59) Gillet, L. C.; Leitner, A.; Aebersold, R. Mass Spectrometry Applied to Bottom-Up Proteomics: Entering the High-Throughput Era for Hypothesis Testing. *Annu. Rev. Anal. Chem.* **2016**, 9, 449-472.
(60) Huang, Y.; Triscari, J. M.; Pasa-Tolic, L.; Anderson, G. A.; Lipton, M. S.; Smith, R. D.; Wysocki, V. H. Dissociation Behavior of Doubly-Charged Tryptic Peptides: Correlation of Gas-Phase Cleavage Abundance with Ramachandran Plots. *J. Am. Chem. Soc.* **2004**, 126, 3034-3035.
(61) Wang, G.; Cole, R. B. Disparity Between Solution-phase Equilibria and Charge State Distributions in Positive-ion Electrospray Mass Spectrometry. *Org. Mass Spectrom.* **1994**, 29, 419-427.
(62) Kaltashov, I. A.; Abzalimov, R. R. Do Ionic Charges in ESI MS Provide Useful Information on Macromolecular Structure? *J. Am. Soc. Mass Spectrom.* **2008**, 19, 1239-1246.
(63) Kelly, M. A.; Vestling, M. M.; Fenselau, C. C.; Smith, P. B. Electrospray Analysis of Proteins: a Comparison of Positive-ion and Negative-ion Mass Spectra at High and Low pH. *Org. Mass Spectrom.* **1992**, 27, 1143-1147.
(64) Bruins, A. P.; Covey, T. R.; Henion, J. D. Ion Spray Interface for Combined Liquid Chromatography/Atmospheric Pressure Ionization Mass Spectrometry. *Anal. Chem.* **1987**, 59, 2642-2646.
(65) Cech, N. B.; Enke, C. G. Relating Electrospray Ionization Response to Nonpolar Character of Small Peptides. *Anal. Chem.* **2000**, 72, 2717-2723.
(66) Kondalaji, S. G.; Khakinejad, M.; Tafreshian, A.; Valentine, S. J. Comprehensive Peptide Ion Structure Studies Using Ion Mobility Techniques: Part 1. An Advanced Protocol for Molecular Dynamics Simulations and Collision Cross-Section Calculation. *J. Am. Soc. Mass Spectrom.* **2017**, 28, 947-959.
(67) Marginean, I.; Znamenskiy, V.; Vertes, A. Charge Reduction in Electrosprays: Slender Nanojets as Intermediates. *J. Phys. Chem. B* **2006**, 110, 6397-6404.
(68) Baker, E. S.; Burnum-Johnson, K. E.; Ibrahim, Y. M.; Orton, D. J.; Monroe, M. E.; Kelly, R. T.; Moore, R. J.; Zhang, X.; Theberge, R.; Costello, C. E.; Smith, R. D. Enhancing bottom-up and top-down proteomic measurements with ion mobility separations. *Proteomics* **2015**, 15, 2766-2776.
(69) Fuller, D. R.; Conant, C. R.; El-Baba, T. J.; Brown, C. J.; Woodall, D. W.; Russell, D. H.; Clemmer, D. E. Conformationally Regulated Peptide Bond Cleavage in Bradykinin. *J. Am. Chem. Soc.* **2018**, 140, 9357-9360.
(70) Rodriquez, C. F.; Orlova, G.; Guo, Y.; Li, X.; Siu, C.-K.; Hopkinson, A. C.; Siu, K. W. M. Gaseous Bradykinin and Its Singly, Doubly, and Triply Protonated Forms: A First-Principles Study. *J. Phys. Chem. B.* **2006**, 110, 7528-7537.
(71) Schneider, B. B.; Douglas, D. J.; Chen, D. D. Y. Collision-Induced Dissociation of Bradykinin Ions in the Interface Region of an ESI-MS. *J. Am. Soc. Mass Spectrom.* **2001**, 12, 772-779.
(72) Schnier, P. D.; Price, W. D.; Jockusch, R. A.; Williams, E. R. Blackbody infrared radiative dissociation of bradykinin and its analogues: Energetics, dynamics, and evidence for salt-bridge structures in the gas phase. *J. Am. Chem. Soc.* **1996**, 118, 7178-7189.
(73) Bjorkqvist, J.; Jamsa, A.; Renne, T. Plasma kallikrein: the bradykinin-producing enzyme. *Thromb. Haemost.* **2013**, 110, 399-407.

(74) Wang, R.; Zenobi, R. Evolution of the Solvent Polarity in an Electrospray Plume. *J. Am. Soc. Mass Spectrom.* **2010**, 21, 378-385.
(75) Zhou, S.; Cook, K. D. Probing Solvent Fractionation in Electrospray Droplets with Laser-Induced Fluorescence of a Solvatochromic Dye. *Anal. Chem.* **2000**, 72, 963-969.
(76) Liigand, P.; Heering, A.; Kaupmees, K.; Leito, I.; Girod, M.; Antoine, R.; Kruve, A. The Evolution of Electrospray Generated Droplets is Not Affected by Ionization Mode. *J. Am. Soc. Mass Spectrom.* **2017**, 28, 2124-2131.
(77) Girod, M.; Dagany, X.; Boutou, V.; Broyer, M.; Antoine, R.; Dugourd, P.; Mordehai, A.; Love, C.; Werlich, M.; Fjeldsted, J.; Stafford, G. Profiling an electrospray plume by laser-induced fluorescence and Fraunhofer diffraction combined to mass spectrometry: influence of size and composition of droplets on charge-state distributions of electrosprayed proteins. *Phys. Chem. Chem. Phys.* **2012**, 14, 9389-9396.
(78) Abraham, M. J.; Murtola, T.; Schulz, R.; Páll, S.; Smith, J. C.; Hess, B.; Lindahl, E. GROMACS: High performance molecular simulations through multi-level parallelism from laptops to supercomputers. *SoftwareX* **2015**, 1–2, 19-25.
(79) Abascal, J. L. F.; Vega, C. A general purpose model for the condensed phases of water: TIP4P/2005. *J. Chem. Phys.* **2005**, 123, 234505.
(80) Vega, C.; de Miguel, E. Surface tension of the most popular models of water by using the test-area simulation method. *J. Chem. Phys.* **2007**, 126, 154707.
(81) Huang, J.; MacKerell, A. D. CHARMM36 all-atom additive protein force field: Validation based on comparison to NMR data. *J. Comput. Chem.* **2013**, 34, 2135-2145.
(82) Lide, D. R. *CRC Handbook of Chemistry and Physics*, 82nd ed.; CRC Press: Boca Raton, London, New York, Washington, 2001.
(83) Calio, P. B.; Li, C. H.; Voth, G. A. Resolving the Structural Debate for the Hydrated Excess Proton in Water. *J. Am. Chem. Soc.* **2021**, 143, 18672-18683.
(84) Lindahl, E. In *Molecular Modeling of Proteins. Methods in Molecular Biology (Methods and Protocols)*; Kukol, A., Ed.; Humana Press: New York, NY, 2015; Vol. 1215, pp 3-26.
(85) Lopez, J. J.; Shukla, A. K.; Reinhart, C.; Schwalbe, H.; Michel, H.; Glaubitz, C. The structure of the neuropeptide bradykinin bound to the human G-protein coupled receptor bradykinin B2 as determined by solid-state NMR spectroscopy. *Angew. Chem.-Int. Edit.* **2008**, 47, 1668-1671.
(86) Konermann, L. Addressing a Common Misconception: Ammonium Acetate as Neutral pH "Buffer" for Native Electrospray Mass Spectrometry. *J. Am. Soc. Mass Spectrom.* **2017**, 28, 1827-1835.
(87) Zhou, S.; Prebyl, B. S.; Cook, K. D. Profiling pH Changes in the Electrospray Plume. *Anal. Chem.* **2002**, 74, 4885-4888.
(88) Malevanets, A.; Consta, S. Variation of droplet acidity during evaporation. *J. Chem. Phys.* **2013**, 138, 184312.
(89) Girod, M.; Dagany, X.; Antoine, R.; Dugourd, P. Relation between charge state distributions of peptide anions and pH changes in the electrospray plume. A mass spectrometry and optical spectroscopy investigation. *Int. J. Mass Spectrom.* **2011**, 308, 41-48.
(90) Gatlin, C. L.; Turecek, F. Acidity Determination in Droplets Formed by Electrospraying Methanol-Water Solutions. *Anal. Chem.* **1994**, 66, 712-718.
(91) Van Berkel, G. J.; Kertesz, V. Using the Electrochemistry of the Electrospray Ion Source. *Anal. Chem.* **2007**, 79, 5511-5520.
(92) Eigen, M. Proton Transfer, Acid-Base Catalysis, and Enzymatic Hydrolysis. *Angew. Chem.-Int. Edit.* **1964**, 3, 1-72.

(93) Rovelli, G.; Jacobs, M. I.; Willis, M. D.; Rapf, R. J.; Prophet, A. M.; Wilson, K. R. A critical analysis of electrospray techniques for the determination of accelerated rates and mechanisms of chemical reactions in droplets. *Chem. Sci.* **2020**, 11, 13026-13043.
(94) Harrison, A. G. Pathways for Water Loss from Doubly Protonated Peptides Containing Serine or Threonine. *J. Am. Soc. Mass Spectrom.* **2012**, 23, 116-123.
(95) Chowdhury, S. K.; Katta, V.; Chait, B. T. Probing Conformational Changes in Proteins by Mass Spectrometry. *J. Am. Chem. Soc.* **1990**, 112, 9012-9013.
(96) Loo, J. A.; Loo, R. R. O.; Udseth, H. R.; Edmonds, C. G.; Smith, R. D. Solvent-induced Conformational Changes of Polypeptides Probed by Electrospray-ionization Mass Spectrometry. *Rapid. Comm. Mass. Spectrom.* **1991**, 5, 101-105.
(97) Dobo, A.; Kaltashov, I. A. Detection of Multiple Protein Conformational Ensembles in Solution via Deconvolution of Charge-State Distributions in ESI MS. *Anal. Chem.* **2001**, 73, 4763-4773.
(98) Hossain, B. M.; Simmons, D. A.; Konermann, L. Do Electrospray Mass Spectra Reflect the Ligand Binding State of Proteins in Solution? *Can. J. Chem.* **2005**, 83, 1953-1960.
(99) Creighton, T. E. *Proteins*; W. H. Freeman & Co: New York, 1993.
(100) Konermann, L.; Rodriguez, A. D.; Liu, J. On the Formation of Highly Charged Gaseous Ions from Unfolded Proteins by Electrospray Ionization. *Anal. Chem.* **2012**, 84, 6798–6804.

For Table of Contents Only